The Astrophysical Journal, 620:1140–1150, 2005 February 20

THE STRENGTHS OF NEAR-INFRARED ABSORPTION FEATURES RELEVANT TO INTERSTELLAR AND PLANETARY ICES

P. A. Gerakines, J. J. Bray, A. Davis, and C. R. Richey
Astro- and Solar-System Physics Program, Department of Physics, University of Alabama at Birmingham, Birmingham, AL 35294-1170; gerak@uab.edu
Received 2004 October 1; accepted 2004 October 29

ABSTRACT

The abundances of ices in planetary environments have historically been obtained through measurements of near-infrared absorption features ($\lambda = 1.0$–2.5 μm), and near-IR transmission measurements of materials present in the interstellar medium are becoming more common. For transmission measurements, the band strength (or absorption intensity) of an absorption feature must be known in order to determine the column density of an ice component. In the experiments presented here, we have measured the band strengths of the near-IR absorption features for several molecules relevant to the study of interstellar icy grain mantles and icy planetary bodies: CO (carbon monoxide), CO_2 (carbon dioxide), C_3O_2 (carbon suboxide), CH_4 (methane), H_2O (water), CH_3OH (methanol), and NH_3 (ammonia). During a vacuum deposition, the sizes of the near-IR features were correlated with that of a studied mid-IR feature whose strength is well known from previous ice studies. These data may be used to determine ice abundances from observed near-IR spectra of interstellar and planetary materials or to predict the sizes of near-IR features in spectral searches for these molecules in astrophysical environments.

Subject headings: astrochemistry — comets: general — ISM: abundances — ISM: molecules — methods: laboratory — molecular data — planets and satellites: general

1. INTRODUCTION

Observations in the mid-infrared spectral region ($\tilde{\nu} = 4000$–400 cm^{-1}; $\lambda = 2.5$–25 μm) have led to the identification of various molecules in the icy mantles that coat the dust grains present in the interstellar medium (ISM). These include firm identifications of H_2O, CO, CO_2, and OCN^- (cyanate ion), CH_3OH, CH_4, and OCS, some reasonable but more tentative identifications of HCOOH (formic acid), $HCOO^-$ (formate ion), H_2CO (formaldehyde), and NH_3, and the absorption features of some uncharacterized species such as large organics, or molecules possibly related to ammonium (Ehrenfreund & Charnley 2000; Whittet 2003; Gibb et al. 2004 and references therein). Observations of spectral features located in the near-infrared spectral region ($\tilde{\nu} = 12,500$–4000 cm^{-1}; $\lambda = 0.8$–2.5 μm) have been widely used to identify ices in the outer solar system. Molecules such as H_2O, CH_4, CO, CO_2, and N_2 have been identified on planetary bodies such as Pluto, Charon, Triton, and Europa (see a recent review by Roush 2001 and observations by, e.g., Cruikshank et al. 1998; Quirico et al. 1999; Buie & Grundy 2000; or Grundy et al. 2003). Cometary nuclei are presumed to have a composition similar to these objects (e.g., Irvine et al. 2000).

In recent years, observations of the ISM have begun to extend into the near-IR spectral region as well. Observations of interstellar material have been made with instruments such as SpeX on the Infrared Telescope Facility (IRTF) telescope (Vacca et al. 2004) and other instruments (e.g., Murakawa et al. 2000; Taban et al. 2003). The instruments designed for the future *James Webb Space Telescope* (*JWST*) call for an increase in fundamental near-IR data. The *JWST* Near Infrared Spectrometer (NIRSpec) will perform observations from 0.6 to 5 μm at spectral resolutions from 100 to 3000, with the primary objective of studying the processes of star formation in the ISM of external galaxies (Rauscher et al. 2004). Calculations of ice abundances in star-forming regions could be accomplished with near-IR data such as ours.

The relative abundances of ice components can provide key pieces of information about the physical and chemical history of the dense cloud in which the ice species reside. Abundances are obtained by observing the absorption features of a molecule arising from its allowed vibrational modes. For unsaturated features with small peak optical depths, the integrated area of an interstellar ice absorption feature scales with the molecule's abundance by a constant factor. This factor is called the strength of the absorption feature, and it is an intrinsic physical parameter of its carrier molecule. As has been shown in many previous studies (e.g., Gerakines et al. 1995; Kerkhof et al. 1999), the IR band strengths of most molecules show various degrees of dependence on environmental factors, including ice temperature, overall ice composition, or the ice's crystalline phase.

The method by which the column densities of interstellar ices are determined from their IR absorption features derives from the Beer-Lambert law. The fraction of light transmitted through an interstellar cloud at wavenumber $\tilde{\nu}$ is given by $T_{\tilde{\nu}} = \exp(-\tau_{\tilde{\nu}})$, where the optical depth ($\tau_{\tilde{\nu}}$) may be expressed as the Beer-Lambert law in the form

$$\tau_{\tilde{\nu}} = \sigma_{\tilde{\nu}} N, \tag{1}$$

where N is the column density of the absorbing molecule (in cm^{-2}) and $\sigma_{\tilde{\nu}}$ is the absorption cross section (in cm^2) at wavenumber $\tilde{\nu}$ (in cm^{-1}). Since N is a constant with respect to $\tilde{\nu}$, equation (1) can be integrated over wavenumber and rearranged in the form

$$N = \frac{\int_i \tau_{\tilde{\nu}}\, d\tilde{\nu}}{A_i}, \tag{2}$$

where

$$A_i = \int_i \sigma_{\tilde{\nu}}\, d\tilde{\nu}, \tag{3}$$

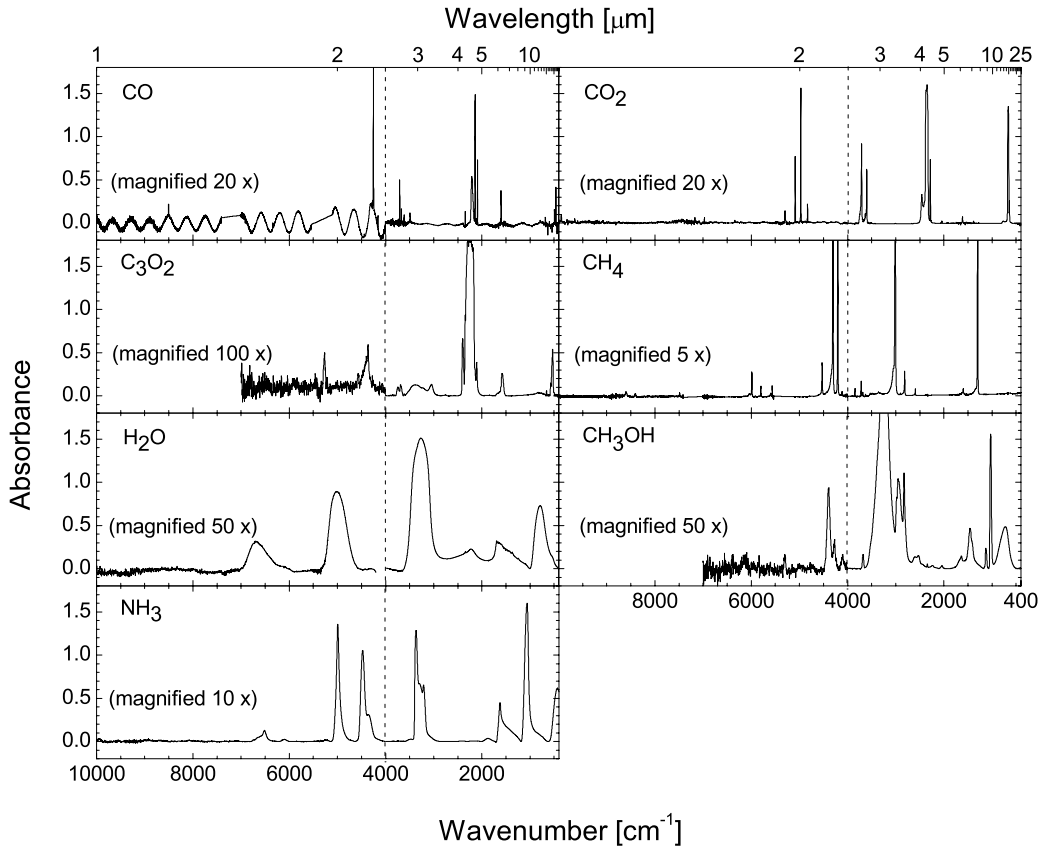

FIG. 1.—Combined near- and mid-IR spectra (10,000–400 cm^{-1}; 1.0–25 μm) of pure samples at 10 K for the seven molecules studied. In each case, the near-IR portion of the spectrum (10,000–4000 cm^{-1}; 1.0–2.5 μm) has been magnified by the amount indicated in the figure. The sinusoidal appearance of the CO near-IR spectrum is due to interference of the spectrometer's IR beam within the sample. Gas-phase H_2O lines from the imperfect spectrometer purge (5540–4100 and 7420–7000 cm^{-1}) have been removed from the near-IR spectra of CO and CH_4. The 10,000–7000 cm^{-1} region has been omitted from the near-IR spectra of C_3O_2 and CH_3OH for clarity, since they are dominated by noise.

and the integrals in equations (2) and (3) are taken over the range of the studied feature *i*. The parameter A_i has many names in the literature, including the "band strength," "integrated cross section," "absolute absorption intensity," or simply "*A*-value" of the IR absorption feature *i*. As expressed above and as is customary in the astrophysical literature, band strengths possess units of cm $molecule^{-1}$, although the physical chemistry literature prefers units such as km $mmol^{-1}$. The IR absorption features of most molecules of astrophysical interest have band strengths in the range from about 10^{-20} to 10^{-16} cm $molecule^{-1}$ (Hudgins et al. 1993; Gerakines et al. 1995; Kerkhof et al. 1999).

Mid-IR absorption features of molecules are the result of their fundamental vibrational modes, combinations of the fundamental modes, and their lowest lying overtones. Near-IR absorptions are generally not due to fundamental vibrations but to higher overtones or combinations of fundamentals and their overtones. As a result, the near-IR features of a certain molecule are usually much weaker than those in the mid-IR. This is demonstrated in Figure 1, where the combined near- and mid-IR spectra of CO, CO_2, C_3O_2, CH_4, H_2O, CH_3OH, and NH_3 are shown. Note that in each case, the near-IR portion of the spectrum ($\tilde{\nu} = 10000–4000$ cm^{-1}; $\lambda = 1.0–2.5$ μm) has been magnified significantly—from 5 to 100 times—in order to display the near- and mid-IR features on similar scales. Laboratory and observational studies typically use the much stronger mid-IR absorption features to make identifications of molecules in astrophysical ices because that they are more sensitive tracers of molecular abundances. However, the mid-IR is not always the best spectral region in which to make astronomical observations. This is the case for reflectance studies within the solar system, since the solar spectrum peaks in the visible range and the Sun emits a much higher flux of near-IR photons than mid-IR photons.

In our laboratory we have the ability to study the composite near-IR and mid-IR spectrum, from 10,000 to 400 cm^{-1} (1.0–25 μm), of our ice samples. This allows us to obtain spectra of the same ice sample in both the near- and mid-IR ranges almost

TABLE 1
MID-INFRARED FEATURES USED IN STRENGTH DETERMINATIONS

Molecule	$\tilde{\nu}$ (cm^{-1})	λ (μm)	A (cm $molecule^{-1}$)	Reference
CO	2092	4.780	1.5×10^{-19}[a]	1
CO_2	3708	2.697	1.4×10^{-18}	1
C_3O_2	3744	2.671	3.8×10^{-18}	2
CH_4	1306	7.657	7.0×10^{-18}	3
	2815	3.552	$(1.9 \pm 0.1) \times 10^{-18}$	4
H_2O	1670	5.988	1.2×10^{-17}	1
CH_3OH	2830	3.534	7.6×10^{-18}	5
NH_3	1070	9.346	1.2×10^{-17}	3

[a] Although this is a feature of ^{13}CO, its band strength is expressed in units of cm per ^{12}CO molecule.

REFERENCES.—(1) Gerakines et al. 1995; (2) Gerakines & Moore 2001; (3) Kerkhof et al. 1999; (4) Determined by scaling the 1306 cm^{-1} (7.657 μm) feature (see text); (5) d'Hendecourt & Allamandola 1986.

TABLE 2
NEAR-IR FEATURES AND BAND STRENGTHS MEASURED AT 10 K

PEAK POSITION		FWHM, $\Delta\tilde{\nu}$		STRENGTH, A	
$\tilde{\nu}$ (cm^{-1})	λ (μm)	(cm^{-1})	VIBRATION MODE	(cm molecule^{-1})	NOTES
CO:[a]					
4159	2.404	3	$2\nu^{13}$ CO	$(2.1 \pm 0.1) \times 10^{-21}$	1
4252	2.352	3	$2\nu^{12}$ CO	$(1.6 \pm 0.1) \times 10^{-19}$	1
6338	1.578	4	$3\nu^{12}$ CO	$(1.5 \pm 0.1) \times 10^{-21}$	1
8504	1.176	8	?	$(3.4 \pm 0.2) \times 10^{-21}$	
CO_2:					
4832	2.070	6	$4\nu_2 + \nu_3$	$(7.8 \pm 0.5) \times 10^{-21}$	1
4971	2.012	7	$\nu_1 + 2\nu_2 + \nu_3$	$(5.4 \pm 0.2) \times 10^{-20}$	1
5087	1.966	7	$2\nu_1 + \nu_3$	$(2.8 \pm 0.1) \times 10^{-20}$	1
6214	1.609	7	$\nu_1 + 4\nu_2 + \nu_3$	$(2.6 \pm 1.8) \times 10^{-22}$	1
6341	1.577	7	$2\nu_1 + 2\nu_2 + \nu_3$	$(8.6 \pm 1.1) \times 10^{-22}$	1
6972	1.434	8	$3\nu_3$	$(2.6 \pm 0.3) \times 10^{-21}$	1
9944	1.006	12	$4\nu_3 + \nu_2$ (?)	$(5.6 \pm 1.9) \times 10^{-21}$	1
C_3O_2:					
4370	2.288	78	$2\nu_3$ (?)	$(1.7 \pm 0.2) \times 10^{-19}$	
4570	2.188	37	$\nu_2 + \nu_3 + \nu_4$ (?)	$(1.7 \pm 0.2) \times 10^{-20}$	
5270	1.898	48	$\nu_2 + 2\nu_3$ (?)	$(5.0 \pm 0.9) \times 10^{-20}$	
CH_4:					
4115	2.430	14	$\nu_2 + 2\nu_4$	$(7.2 \pm 0.1) \times 10^{-20}$	1
4202	2.380	9	$\nu_1 + \nu_4$	$(1.6 \pm 0.1) \times 10^{-18}$	1
4300	2.326	7	$\nu_3 + \nu_4$	$(3.4 \pm 0.1) \times 10^{-18}$	1
4528	2.208	9	$\nu_2 + \nu_3$	$(4.5 \pm 0.1) \times 10^{-19}$	1
5565	1.797	5	$\nu_3 + 2\nu_4$	$(6.8 \pm 0.1) \times 10^{-20}$	1
5800	1.724	8	$\nu_2 + \nu_3 + \nu_4$	$(1.3 \pm 0.1) \times 10^{-19}$	1
5987	1.670	7	$2\nu_3$	$(3.8 \pm 0.1) \times 10^{-19}$	1
7487	1.336	11	$\nu_2 + 2\nu_3$	$(5.3 \pm 0.1) \times 10^{-20}$	1
8405	1.190	30	$[\nu_1] + [\nu_1] + [\nu_4] + [\nu_4]$	...	2
8588	1.164	42	$2\nu_3 + 2\nu_4$	$(5.4 \pm 0.1) \times 10^{-20}$	1
8780	1.139	17	$\nu_2 + 2\nu_3 + \nu_4$	$(2.0 \pm 0.1) \times 10^{-20}$	1
9060	1.104	28	$3\nu_3$	$(2.1 \pm 0.2) \times 10^{-20}$	3
H_2O:					
5040	1.984	408	$\nu_2 + \nu_3$	$(1.2 \pm 0.1) \times 10^{-18}$	
6684	1.496	520	$2\nu_3$	$(8.8 \pm 1.0) \times 10^{-19}$	
CH_3OH:					
4280	2.336	34	?	$(8.0 \pm 0.9) \times 10^{-20}$	
4400	2.273	72	?	$(8.7 \pm 0.7) \times 10^{-19}$	
NH_3:					
4474	2.235	94	$\nu_1 + \nu_2$ (?)	$(8.7 \pm 0.3) \times 10^{-19}$	
4993	2.002	68	$\nu_1 + \nu_4$ (?)	$(8.1 \pm 0.4) \times 10^{-19}$	
6099	1.640	107	$\nu_1 + \nu_2 + \nu_4$ (?)	$(2.8 \pm 0.5) \times 10^{-20}$	
6515	1.535	118	$2\nu_1$ (?)	$(3.9 \pm 0.3) \times 10^{-20}$	

NOTES.—(1) Vibrational mode assignment from Calvani et al. (1992) and Quirico & Schmitt (1997). (2) Combination of dual-phonon modes (Calvani et al. 1992; Quirico & Schmitt 1997). (3) Vibrational mode assignment from Grundy et al. (2002).
[a] All ^{12}CO and ^{13}CO band strengths are expressed in units of cm per ^{12}CO molecule.

simultaneously, and thus spectral characteristics in both regions may be studied for any material of interest. Ongoing work from our laboratory (Cook et al. 2002; Richey et al. 2004) has focused on measuring the near-IR spectra of thick ($\sim$50 μm) ices that have been highly processed by UV photons.

In this study we present the near-IR band strengths of CO, CO_2, C_3O_2, CH_4, H_2O, CH_3OH, and NH_3. H_2O, CH_3OH, CO, CO_2, and CH_4 are confirmed components of interstellar icy grain mantles, with H_2O dominating most interstellar ice environments (e.g., Whittet 2003). These are also ice species found in many icy planetary bodies, including comets and icy moons such as Europa or Triton (e.g., Roush 2001). Extensive searches for the absorption features of NH_3 ice in interstellar and planetary environments have been performed, with some varied evidence for their presence (e.g., Gibb et al. 2001; Gürtler et al. 2002; Taban et al. 2003). The carbon suboxide molecule (C_3O_2) is of interest to both interstellar and planetary astronomers because it is formed from solid CO in environments affected by energetic processing such as particle irradiation by cosmic rays or magnetospheric particles, or by ultraviolet photolysis (Huntress et al. 1991; Brucato et al. 1997; Gerakines & Moore 2001).

The near-IR band strengths of these molecules were obtained in pure ice samples at 10 K by correlating the growths of the near-IR features with those in the mid IR over the course of long, slow deposits of these materials from the gas phase. Future work (currently in the preliminary phase) will include studies of near- and mid-IR reflectance spectra as well as the calculations of ice optical constants in these spectral ranges.

2. EXPERIMENTAL METHODS

The ice creation methods and the experimental system used in this study are very similar to those in previous studies by, e.g.,

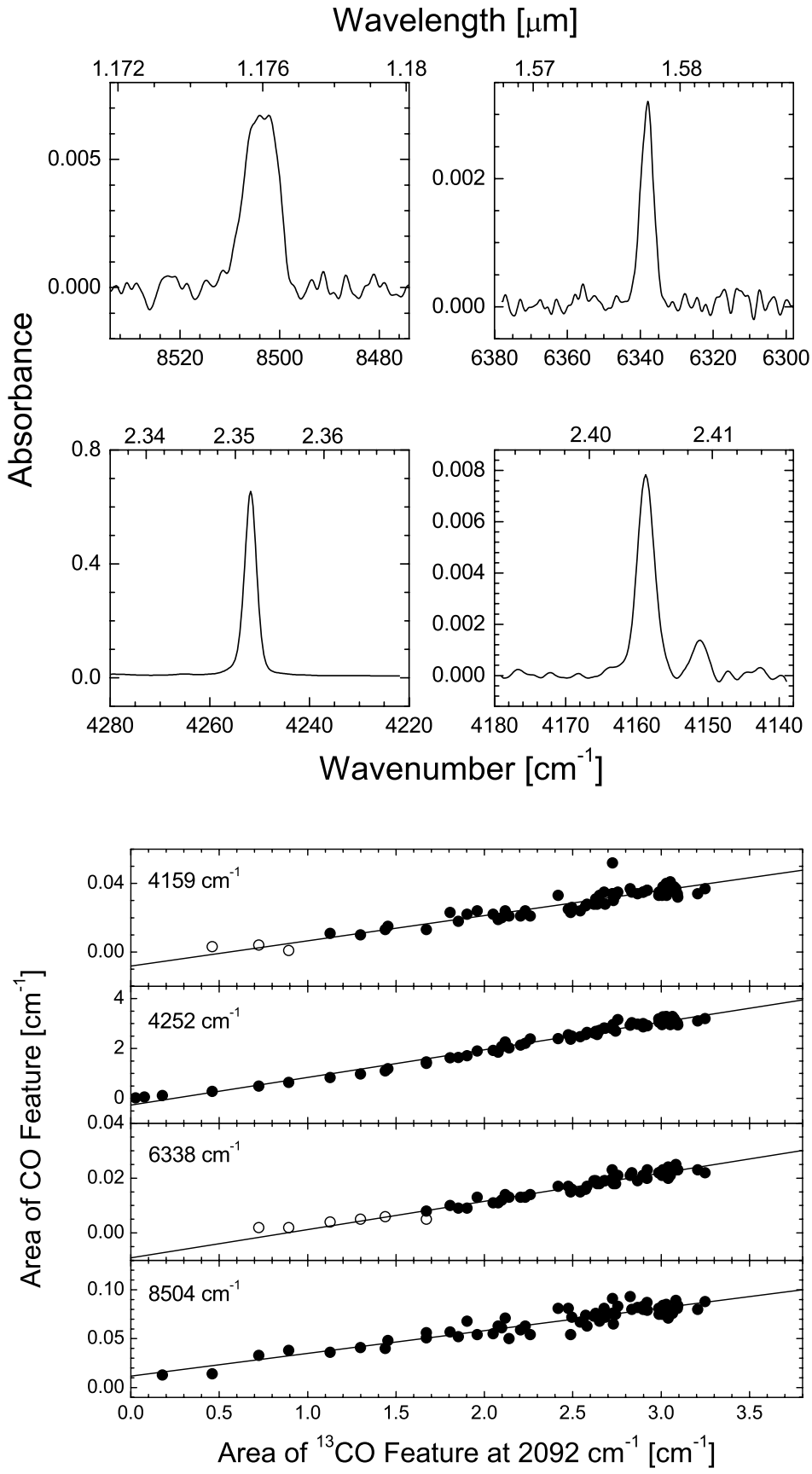

FIG. 2.—*Top*: Selected near-IR absorbance spectra of an 18 μm thick CO ice at 10 K for the regions surrounding the features studied. *Bottom*: Integrated areas (in cm^{-1}) of CO near-IR features plotted vs. the area (in cm^{-1}) of the ^{13}CO feature at 2092 cm^{-1} (4.780 μm) during deposition at 10 K. *Solid lines*: Linear fits to the solid symbols. Data points plotted with empty symbols were omitted from the fits (see text).

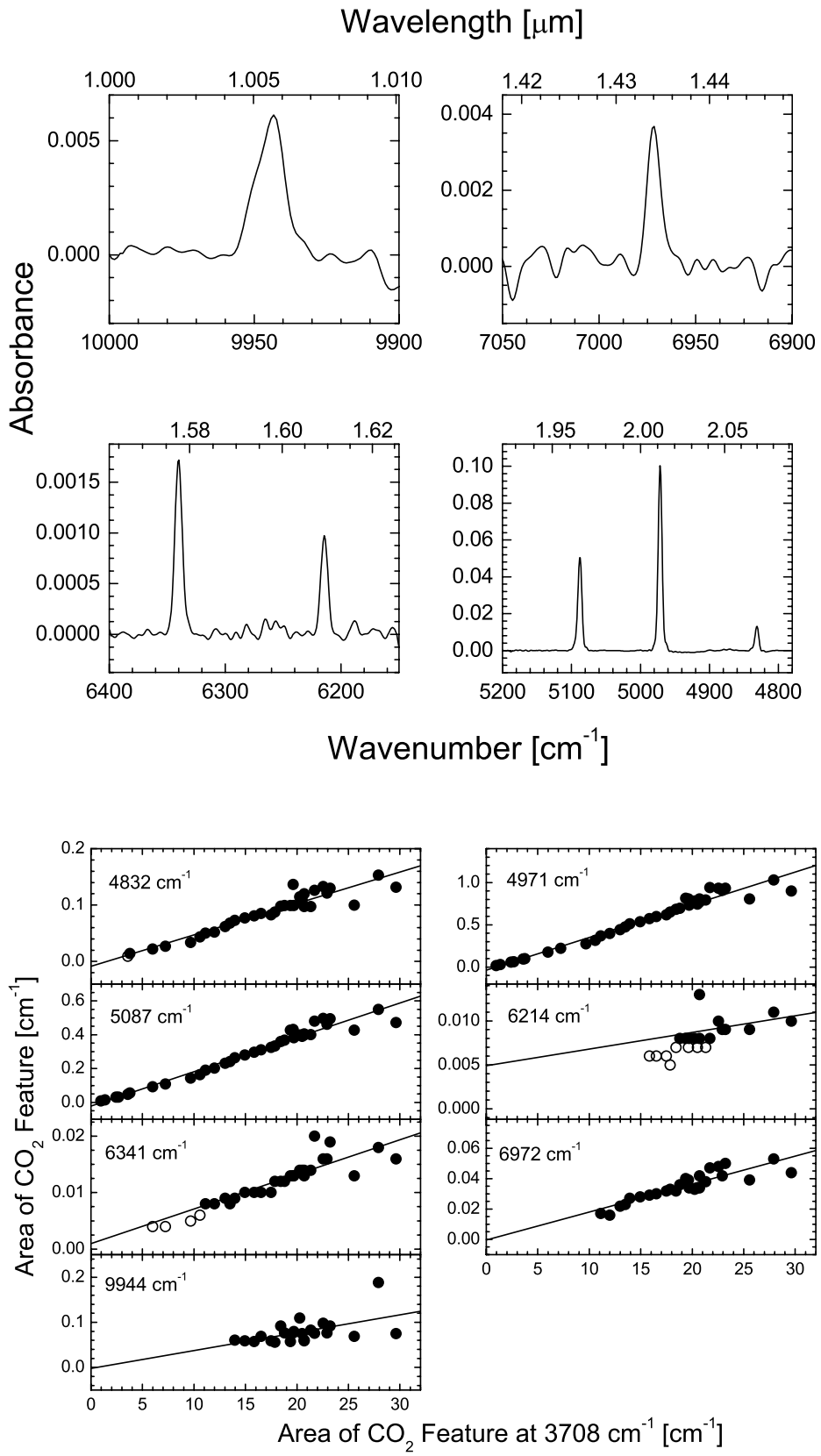

FIG. 3.—*Top*: Selected regions of the near-IR absorbance spectrum of an ~14 μm thick CO_2 ice at 10 K for the regions surrounding the features studied. *Bottom*: Integrated areas (in cm^{-1}) of CO_2 near-IR features plotted vs. the area (in cm^{-1}) of the CO_2 feature at 3708 cm^{-1} (2.697 μm) during deposition at 10 K. Lines and symbols have the same meaning as in Fig. 2.

Hudgins et al. (1993), Gerakines et al. (1995, 2000), Kerkhof et al. (1999), and Gerakines & Moore (2001).

Gases are prepared inside a vacuum manifold and vapor-condensed onto an infrared transmitting substrate (CsI) mounted in the vacuum chamber ($P \approx 3 \times 10^{-6}$ mm hg at room temperature). The substrate is cooled by a closed-cycle helium refrigerator (Air Products) to a temperature of 10 K. The temperature of the substrate is continuously monitored by a chromel-Au thermocouple and is adjustable by a resistive heater element up to room temperature. The chamber that houses the substrate is accessible to laboratory instruments through four ports. Two of these ports are have windows composed of KBr, allowing the transmission of the infrared beam of the spectrometer. One of the ports contains a window composed of MgF_2 to enable ultraviolet photolysis of the ice samples (this option was not used for the experiments described in this paper), while the fourth port has a glass window and is used for visual monitoring.

The sample chamber is positioned within the sample compartment of an FTIR spectrometer (ThermoMattson Infinity Gold) so that the spectrometer's IR beam passes through the KBr windows and CsI substrate. The spectrometer system is capable of automatic switching between the appropriate configurations of sources, detectors, and beam splitters that allow the acquisition of spectra in either the near-IR or mid-IR without breaking the dry air purge. This feature allows the measurement of spectra in each of these two spectral regions for the same ice sample in a single experiment. Near-IR spectra were obtained over the range from 10,000 to 3500 cm^{-1} ($\lambda = 1.0$–2.9 μm) and mid-IR spectra from 4500 to 400 cm^{-1} ($\lambda = 2.2$–25 μm). Some overlap between these ranges allows for cross-calibration of common features as well as for the concatenation of spectra. The spectra of H_2O, NH_3, CH_3OH, CO_2, and C_3O_2 were obtained with a resolution of 4 cm^{-1}. The IR spectra of CH_4 and CO were taken at a resolution of 1 cm^{-1}. Absorbance spectra ($\alpha_{\tilde{\nu}}$) were calculated from the transmission data ($T_{\tilde{\nu}}$) by using the relationship $\alpha_{\tilde{\nu}} = -\log_{10} T_{\tilde{\nu}}$ (note that $\tau_{\tilde{\nu}} = \alpha_{\tilde{\nu}} \ln 10$).

A bulb containing the gas to be condensed was prepared on a separate vacuum manifold and then connected to the high-vacuum system by a narrow tube through a needle valve, which controlled the gas flow into the high-vacuum system. The tube is positioned to release the gases just in front of the cold substrate window. Gases were deposited at a rate of about 1–5 μm hr^{-1}. Most deposits spanned several days in order to create ices thick enough to display detectable near-IR absorptions. No significant contamination by background gases in the vacuum system (dominated by H_2O) was observed, supported by the lack of bulk H_2O features in the IR spectra of the non-H_2O samples. However, some small amounts of H_2O may be isolated within the CO and CO_2 samples, as indicated by sharp features near 3400 and 1600 cm^{-1} ($\lambda = 2.9$ and 6.3 μm) in the mid-IR spectrum shown in Figure 1. As indicated by Gerakines et al. (1995), the band strengths of CO and CO_2 are not significantly affected by small relative amounts of H_2O in an ice sample.

It is important to note that ice samples created in this manner at 10 K are expected to be amorphous rather than crystalline. The amorphous nature of our samples was supported by the IR spectra that were recorded during each sample deposit (see Fig. 1).

The gases used and their purities are as follows: CO (Matheson, 99.9%), CO_2 (Matheson, 99.8%), C_3O_2 (synthesized), CH_4 (Matheson, 99+%), H_2O (distilled by freeze-thaw cycles under vacuum), CH_3OH (distilled by freeze-thaw cycles under vacuum), and NH_3 (Matheson, 99+%). H_2O and CH_3OH were purified by freezing with liquid N_2 under vacuum and pumping away the more volatile gases while thawing. Carbon suboxide was prepared as described in detail by Gerakines & Moore (2001), who followed the method of Miller & Fateley (1964) to dehydrate malonic acid in the presence of phosphorus pentoxide (P_2O_5; a dessicant). To summarize: the gases produced by heating malonic acid to 413 K (H_2O, CO_2, acetic acid, and C_3O_2) were collected in a liquid N_2 trap, and the C_3O_2 was distilled by thermal transfer into a new bulb in the vacuum manifold.

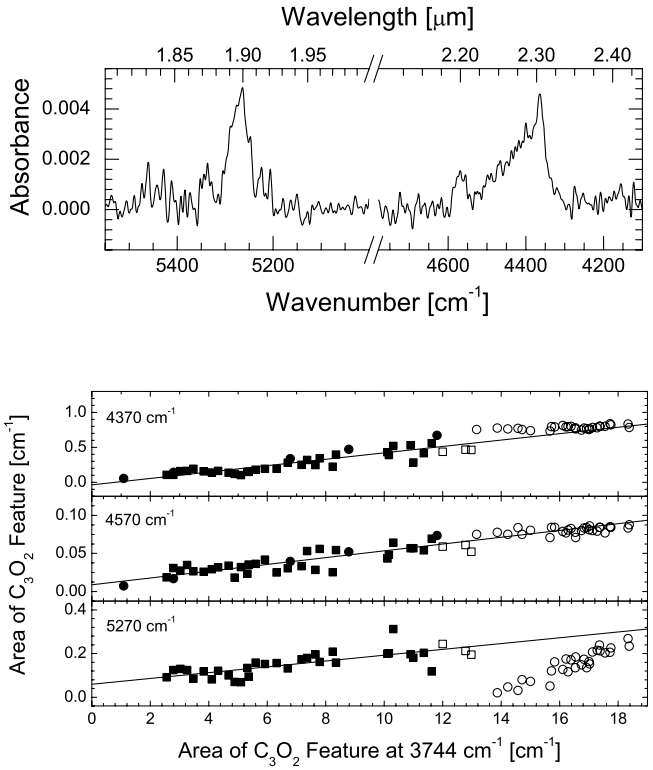

FIG. 4.—*Top*: Selected regions of the near-IR absorbance spectrum of a thick C_3O_2 sample at 10 K. *Bottom*: Integrated areas (in cm^{-1}) of C_3O_2 near-IR features plotted vs. the area (in cm^{-1}) of the C_3O_2 feature at 3700 cm^{-1} (2.703 μm) during deposition at 10 K. Data points plotted as squares were measured from a separate deposit experiment from those plotted with circles. Otherwise, the lines and symbols have the same meaning as in Fig. 2.

3. RESULTS

The spectra of pure CO, CO_2, C_3O_2, CH_4, H_2O, CH_3OH, and NH_3 were collected in the near-IR region from 10,000 to 3500 cm^{-1} (1.0–2.9 μm) and the mid-IR region from 4500 to 400 cm^{-1} (2.2–25 μm) during the slow growth of films at 10 K. Figure 1 displays representative concatenated spectra (10,000–400 cm^{-1}; 1.0–25 μm) of these ice samples. The near-IR regions in Figure 1 have been magnified for direct comparison to the mid-IR region. Band strengths were measured by observing the rate of growth of a near-IR feature in relation to that of a stronger feature in the mid-IR, as described below. The mid-IR features used and their band strengths are listed in Table 1. The near-IR features observed in the spectra and their calculated band strengths are listed in Table 2. Figures 2–8 display the selected near-IR regions of the studied spectra and the curves of growth of the near-IR features.

The integrated absorbance of each feature (in units of cm^{-1}) was measured by integrating between baseline points on either side of the feature, assuming a linear shape to the baseline underneath each feature. The error in the feature areas was estimated by integrating across the same limits when no feature

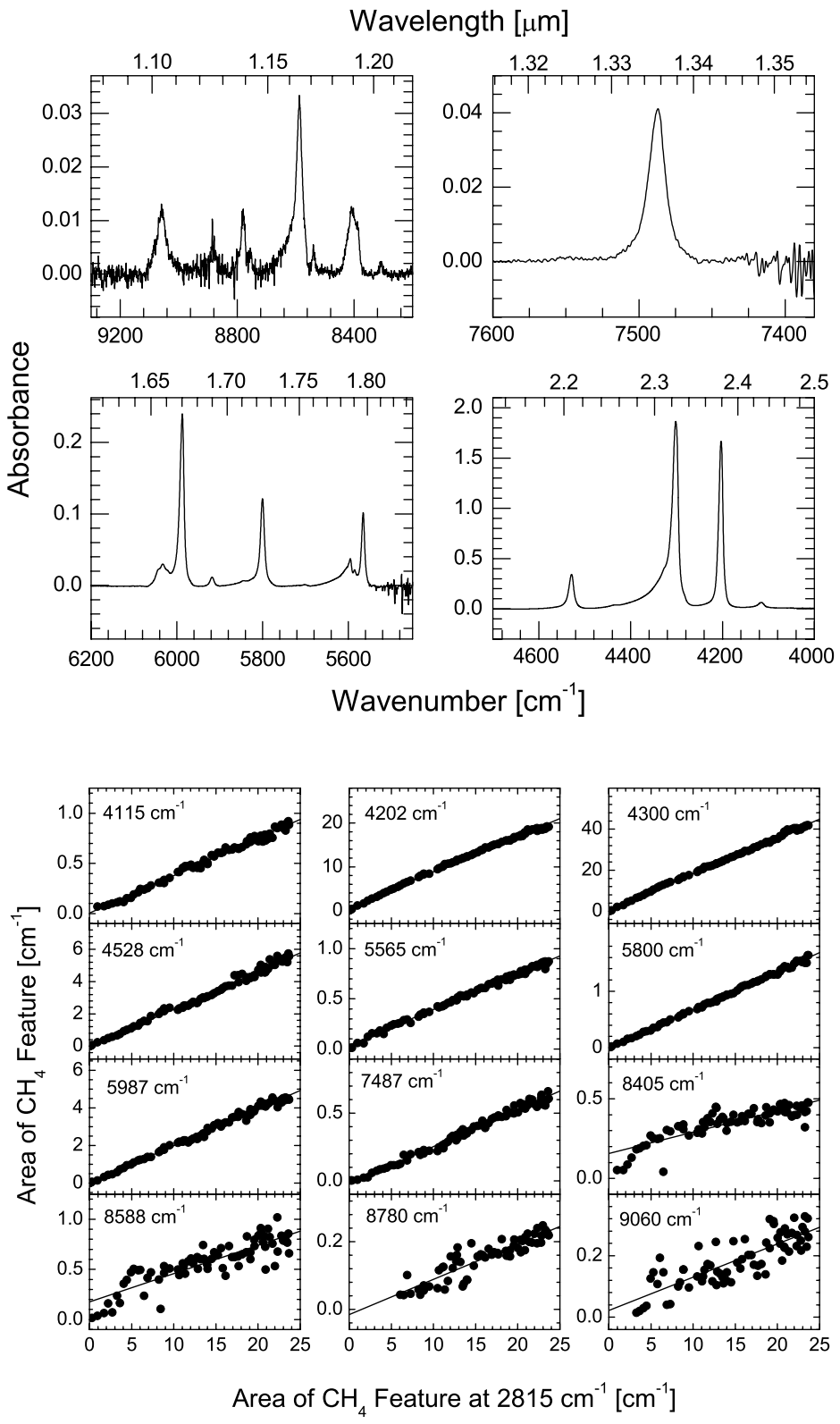

FIG. 5.—*Top*: Selected regions of the near-IR absorbance spectrum of a thick CH_4 sample at 10 K. *Bottom*: Integrated areas (in cm^{-1}) of CH_4 near-IR features plotted vs. the area (in cm^{-1}) of the CH_4 feature at 2815 cm^{-1} (3.552 μm) during deposition at 10 K. Lines and symbols have the same meaning as in Fig. 2.

was apparent above the noise level in the infrared spectrum. For narrow features ($\Delta\tilde{\nu} \lesssim 10$ cm^{-1}), the errors were found to be about 0.005–0.01 cm^{-1}, and larger for wider features (in direct proportion to the width). For this reason, any areas with measured values below about 0.008 cm^{-1} were omitted from the fitting procedure (these points are plotted as open symbols in Figs. 2–8).

To determine the relative strengths of two absorption features for a single molecule, we have examined the relationship between the areas of these bands as the ice is grown. In principle,

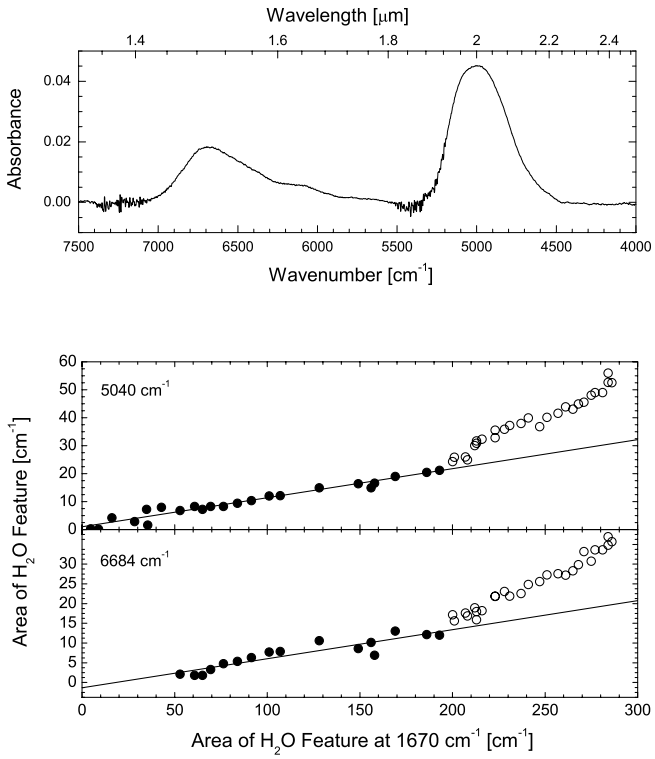

FIG. 6.—*Top*: Near-IR absorbance spectrum of an ~11 μm thick H_2O ice at 10 K in the range of 7500–4000 cm^{-1} (1.333–2.5 μm), displaying the features at 6684 and 5040 cm^{-1} (1.496 and 1.984 μm). *Bottom*: Integrated areas (in cm^{-1}) of H_2O near-IR features plotted vs. the area (in cm^{-1}) of the H_2O feature at 1670 cm^{-1} (5.988 μm) during deposition at 10 K. Lines and symbols have the same meaning as in Fig. 2.

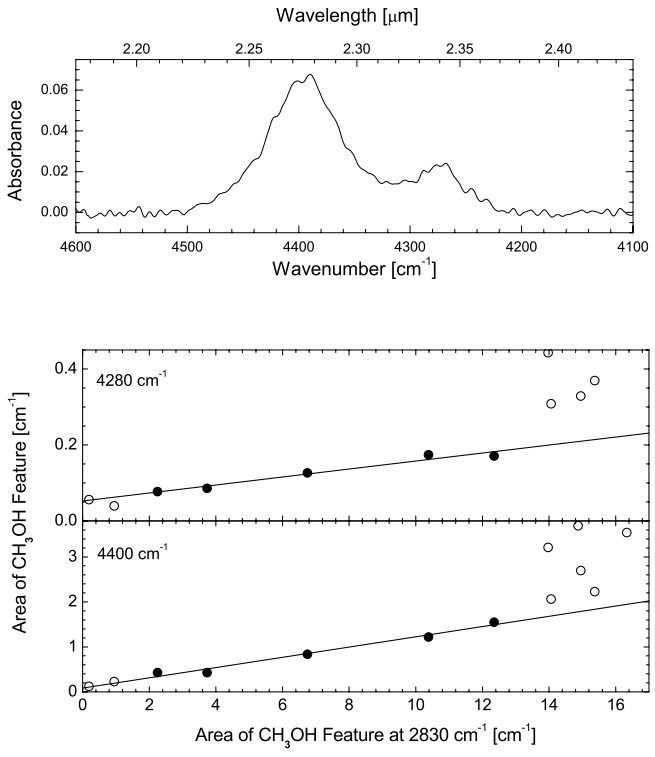

FIG. 7.—*Top*: Near-IR absorbance spectrum of a thick CH_3OH sample at 10 K. *Bottom*: Integrated areas (in cm^{-1}) of CH_3OH near-IR features plotted vs. the area (in cm^{-1}) of the CH_3OH feature at 2830 cm^{-1} (3.534 μm) during deposition at 10 K. Lines and symbols have the same meaning as in Fig. 2.

one could merely measure a single ice spectrum and determine the relative strengths of any two features by taking the ratio of their areas. However, since the near-IR features are much weaker than those in the mid-IR (typically 10–100 times smaller; see Fig. 1), errors in their measured areas are relatively much higher. By monitoring the relationship between two given absorption features over the course of a slow deposit, the systematic errors involved in measuring the areas of the near-IR features are significantly reduced.

For optically thin ice absorptions, we expect that depositing a certain number of molecules will cause a linear increase the areas of both features, where each increase is proportional to that feature's band strength; see equation (2). Hence, the initial trend in a plot of feature area versus feature area should be a straight line, whose slope corresponds to the ratio of the band strengths. Multiplying this ratio by the known band strength of the mid-IR feature (Table 1), the near-IR band strength is obtained. The experimental errors in near-IR band strengths were obtained by multiplying the standard deviations in the best-fitting slopes by the mid-IR band strength. Values resulting from the trends displayed in Figures 2–8 are listed in Table 2.

In the cases of CO, CO_2, and CH_4, the scaling process was complicated by the fact that the fundamental features are extremely sharp and become saturated very quickly during the deposit. For CO (Fig. 2), the absorption due to its fundamental vibration at 2137 cm^{-1} (4.679 μm) becomes too large to be useful after only short deposition times. As a result, we have used the absorption feature of ^{13}CO at 2092 cm^{-1} (4.780 μm) to scale the ^{12}CO and ^{13}CO near-IR features. The strength of 1.5×10^{-19} cm per ^{12}CO molecule was used for the 2092 cm^{-1} (4.780 μm) feature, taking the band strength of the ^{13}CO feature from Gerakines et al. (1995) and scaling by the terrestrial ratio of $^{12}C/^{13}C$ of 87. For CO_2, the combination mode at 3708 cm^{-1} (2.697 μm) was used to scale the near-IR features. For CH_4 (Fig. 5), the absorptions due to fundamental modes at 3009 and 1306 cm^{-1} (3.323 and 7.657 μm) become too strong to be useful after only short timescales as well. Because of this, the near-IR features were scaled by the absorption feature located at 2815 cm^{-1} (3.552 μm), which is due to its $\nu_2 + \nu_4$ vibration mode. In order to do this, we first determined the band strength for the 2815 cm^{-1} (3.552 μm) feature to be $A = (1.9 \pm 0.1) \times 10^{-18}$ cm $molecule^{-1}$ by scaling it by the ν_2 fundamental mode at 1306 cm^{-1} ($\lambda = 7.657$ μm; $A = 7.0 \times 10^{-18}$ cm $molecule^{-1}$; Kerkhof et al. 1999) in the spectrum of a thin sample. The 8405 cm^{-1} (1.190 μm) feature of CH_4 displayed a peculiar growth curve, with no discernible linear trend. Hence, no band strength is listed for this feature in Table 2.

As observed in Figures 2–8, the trends are initially linear for the ices we have studied. In some cases, the mid-IR feature used for the *x*-axis becomes so large that its curve of growth becomes nonlinear (the change in feature area no longer responds linearly to the increase in the number of molecules). In these cases, the nonlinear portions of the data set were omitted from our fitting process (omitted data points are plotted as open symbols in Figs. 2–8). It may be interesting to note that the nonlinear parts of the curve are not always identical from experiment to experiment. This is especially clear in the two separate deposits of C_3O_2 (Fig. 4), H_2O (Fig. 6), and NH_3 (Fig. 8). This may suggest that ice deposition rates or other characteristics of a single experiment can significantly alter the physical properties of the ice under study, especially when ices are thicker than about 10 μm. This particular issue has

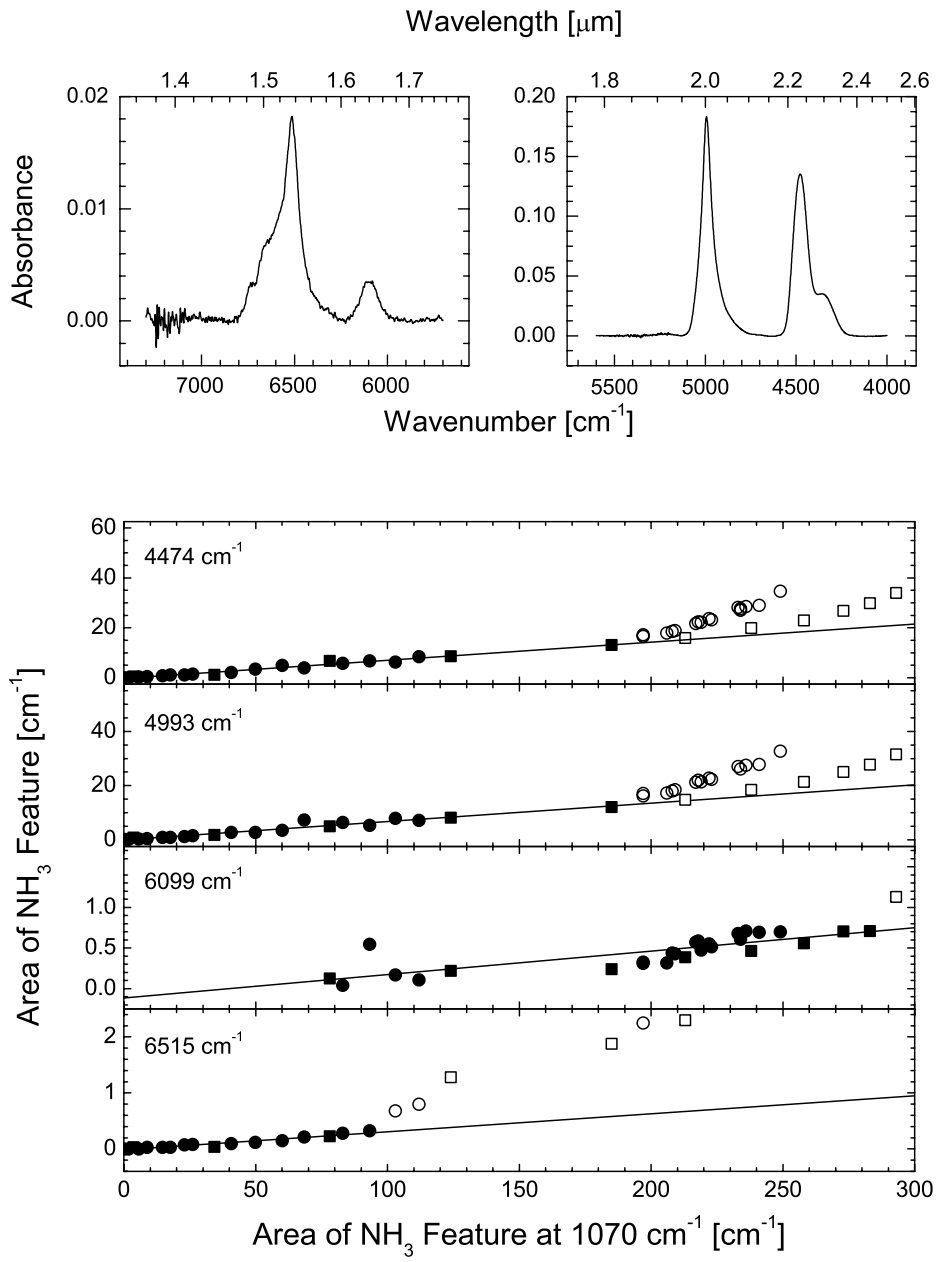

FIG. 8.—*Top*: Selected regions of the near-IR absorbance spectrum of a thick NH_3 sample at 10 K. *Bottom*: Integrated areas (in cm^{-1}) of NH_3 near-IR features plotted vs. the area (in cm^{-1}) of the NH_3 feature at 1070 cm^{-1} (9.346 μm) during deposition of NH_3 at 10 K. Data points plotted as squares were measured from a separate deposit experiment from those plotted with circles. Otherwise, lines and symbols have the same meaning as in Fig. 2.

been discussed in detail previously by Quirico & Schmitt (1997).

4. COMPARISON TO PREVIOUS STUDIES

Taban et al. (2003) have published values for some of the same near-IR band strengths of pure H_2O, NH_3, and CH_3OH ices at low temperatures. In general, we find our values to be in excellent agreement with theirs. They quote $A = 1.1 \times 10^{-18}$ cm molecule^{-1} for the H_2O feature near 5000 cm^{-1} (2.0 μm), which is in full agreement with our experimentally determined value of $(1.2 \pm 0.1) \times 10^{-18}$ cm molecule^{-1}. For NH_3, they find a value of $A = 9.7 \times 10^{-19}$ cm cm molecule^{-1} for the band near 4478 cm^{-1} (2.233 μm), for which we find $A = (8.7 \pm 0.3) \times 10^{-19}$ cm cm molecule^{-1}. For CH_3OH, they measure $A = 5.9 \times 10^{-19}$ cm cm molecule^{-1} for the feature near 4395 cm^{-1} (2.275 μm), which is also in good agreement with our measured value of $(8.7 \pm 0.7) \times 10^{-19}$ cm cm molecule^{-1} for the 4400 cm^{-1} (2.273 μm) feature observed here.

Quirico & Schmitt (1997) published absorption coefficients (the fraction of intensity absorbed per unit thickness of the sample) of the near-IR features of pure CO, CO_2, and CH_4 for use in planetary ice studies. The absorption coefficient allows one to calculate the thickness of a sample from the absorbance value at the peak of a feature. It is not necessarily straightforward to compare band strengths with absorption coefficients for ice samples prepared in separate laboratories using different techniques, since one must take into account the densities of the samples in order to connect column densities to thicknesses. Ice samples in the Quirico & Schmitt (1997) study were created in a closed cell and not by vapor deposit. For the sake of a

TABLE 3
COLUMN DENSITIES AND PREDICTED NEAR-IR OPTICAL DEPTHS OF INTERSTELLAR ICES

Parameter	W33A	NGC 7538 IRS 9	Elias 16	Sgr A*
CO:				
N	8.8×10^{17}	1.2×10^{18}	6.3×10^{17}	$<2 \times 10^{17}$
τ(2.352 μm)	0.05	0.06	0.03	<0.01
CO_2:				
N	1.4×10^{18}	1.7×10^{18}	4.5×10^{17}	1.8×10^{17}
τ(1.966 μm)	0.006	0.007	0.002	<0.001
τ(2.012 μm)	0.01	0.01	0.004	0.001
CH_4:				
N	1.7×10^{17}	1.5×10^{17}	...	2.6×10^{16}
τ(2.326 μm)	0.08	0.07	...	0.01
τ(2.380 μm)	0.03	0.03	...	0.005
H_2O:				
N	1.1×10^{19}	7.5×10^{18}	2.5×10^{18}	1.3×10^{18}
τ(1.496 μm)	0.02	0.01	0.004	0.002
τ(1.984 μm)	0.03	0.02	0.007	0.004
CH_3OH:				
N	2.0×10^{17}	3.8×10^{17}	$<8 \times 10^{16}$	$<5 \times 10^{16}$
τ(2.273 μm)	0.02	0.005	<0.01	<0.006
τ(2.336 μm)	0.005	<0.001	<0.002	<0.001

NOTES.—Column densities (N) have units of cm^{-2} (Gibb et al. 2000). Optical depths have been calculated from the listed column densities, using width and strength data listed in Table 2.

comparison to our study, one must make the rather unsafe assumption that the ice densities and spectral profiles of our samples are identical to theirs (they most likely are not identical). In this case, the band strengths of any two features for a given molecule should scale in the same manner as their absorption coefficients. Taking the ratios of band strengths from Table 2 for pairs of CO, CO_2, and CH_4 features and comparing them to the ratios of their reported absorption coefficients Quirico & Schmitt (1997), we find that some agree quite well (to within a few percent), but most agree only to within a factor of 2 or so.

Taban et al. (2003) find that the near-IR spectrum of the line of sight toward the high-mass protostar W33A is consistent with the known abundances of H_2O, CH_3OH, and CO as derived from mid-IR data. They claim the detection of the near-IR features of CH_3OH near 4400 cm^{-1} (2.273 μm) with an optical depth of about 0.014.

Based on our laboratory data, one should be able to predict the optical depths of near-IR ice absorptions that could be investigated in various astrophysical objects. Using the widths and strengths for the two strongest near-IR features of our samples, we have estimated the optical depths for some well-studied lines of sight in the ISM (e.g., Gerakines et al. 1999; Gibb et al. 2000). These estimates are listed in Table 3. Although pure ices at 10 K may not reflect the most realistic cases for these objects, previous work (Gerakines et al. 1995; Kerkhof et al. 1999) does suggest that the band strengths of most molecules studied to date do not vary by more than a factor of 2 or so according to composition or to temperature. It should be noted that the strengths of a certain molecule's absorption features do vary by large amounts when different crystalline states are considered, but interstellar ices are presumed to be amorphous (e.g., Whittet 2003).

5. SUMMARY AND FUTURE WORK

In this paper, we have shown that the near-IR band strengths (or "absorption intensities") for molecules of interest to both interstellar and planetary astronomers may be determined through correlations to their better known mid-IR characteristics. By correlating the growth of near-IR and mid-IR absorption features for molecules at low temperature, we have calculated the absorption strengths for the near-IR features of CO, CO_2, C_3O_2, CH_4, H_2O, CH_3OH, and NH_3. These strengths may be used to determine the column densities of these molecules in the interstellar dense cloud or other environments from observed transmission data.

This is the first paper in a series of near- and mid-IR correlation studies of ice samples of astrophysical interest. Future work currently in preparation in our laboratory will involve the calculation of ice optical constants for use in particle scattering models as well as reflectance studies for use in the direct interpretation of planetary observations of reflected sunlight. We will also investigate the effects, if any, of ice composition on the near-IR band strengths as well as the differences between the near-IR band strengths of crystalline and amorphous ices.

P. A. G. gratefully acknowledges laboratory start-up funds from the University of Alabama at Birmingham, financial support through NASA grant number NNG04GA63A, and many conversations with Marla Moore and Reggie Hudson, who kindly provided comments on an early version of this manuscript.

REFERENCES

Brucato, J. R., Palumbo, M. E., & Strazzulla, G. 1997, Icarus, 125, 135
Buie, M. W., & Grundy, W. M. 2000, Icarus, 148, 324
Calvani, P., Cunsolo, S., Lupi, S., & Nucara, A. 1992, J. Chem. Phys., 96, 7372
Cook, A. M., Gerakines, P. A., & Saperstein, E. 2002, BAAS, 34, 908
Cruikshank, D. P., et al. 1998, Icarus, 135, 389
d'Hendecourt, L. B., & Allamandola, L. J. 1986, A&AS, 64, 453
Ehrenfreund, P., & Charnley, S. B. 2000, ARA&A, 38, 427
Gerakines, P. A., & Moore, M. H. 2001, Icarus, 154, 372
Gerakines, P. A., Moore, M. H., & Hudson, R. L. 2000, A&A, 357, 793
Gerakines, P. A., Schutte, W. A., Greenberg, J. M., & van Dishoeck, E. F. 1995, A&A, 296, 810
Gerakines, P. A., et al. 1999, ApJ, 522, 357

Gibb, E. L., Whittet, D. C. B., Boogert, A. C. A., & Tielens, A. G. G. M. 2004, ApJS, 151, 35
Gibb, E. L., Whittet, D. C. B., & Chiar, J. E. 2001, ApJ, 558, 702
Gibb, E. L., et al. 2000, ApJ, 536, 347
Grundy, W. M., Schmitt, B., & Quirico, E. 2002, Icarus, 155, 486
Grundy, W. M., Young, L. A., & Young, E. F. 2003, Icarus, 162, 222
Gürtler, J., Klaas, U., Henning, T., Ábrahám, P., Lemke, D., Schreyer, K., & Lehmann, K. 2002, A&A, 390, 1075
Hudgins, D. M., Sandford, S. A., Allamandola, L. J., & Tielens, A. G. G. M. 1993, ApJS, 86, 713
Huntress, W. T., Allen, M., & Delitsky, M. 1991, Nature, 352, 316
Irvine, W. M., Schloerb, F. P., Crovisier, J., Fegley, B., & Mumma, M. J. 2000, in Protostars and Planets IV, ed. V. Mannings, A. P. Boss, & S. S. Russell (Tucson: Univ. Arizona Press), 1159
Kerkhof, O., Schutte, W. A., & Ehrenfreund, P. 1999, A&A, 346, 990
Miller, F. A., & Fateley, W. G. 1964, Spectrochim. Acta, 20, 253
Murakawa, K., Tamura, M., & Nagata, T. 2000, ApJS, 128, 603
Quirico, E., Doute, S., Schmitt, B., de Bergh, C., Cruikshank, D. P., Owen, T. C., Geballe, T. R., & Roush, T. L. 1999, Icarus, 139, 159
Quirico, E., & Schmitt, B. 1997, Icarus, 127, 354
Rauscher, B. J., Figer, D. F., Hill, R. J., Jakobsen, P. J., Moseley, S. H., Regan, M. W., & Strada, P. 2004, AAS Meeting, 204, 1102
Richey, C. R., Underwood, R. A., & Gerakines, P. A. 2004, Lunar Planet. Sci. Conf., 35, 1450
Roush, T. L. 2001, J. Geophys. Res., 106, 33315
Taban, I. M., Schutte, W. A., Pontoppidan, K. M., & van Dishoeck, E. F. 2003, A&A, 399, 169
Vacca, W. D., Cushing, M. C., & Simon, T. 2004, ApJ, 609, L29
Whittet, D. C. B. 2003, Dust in the Galactic Environment (2nd ed; Bristol: IOP)